Electronic Supplementary Information (ESI) for *Dalton Transactions*

Single Molecule Magnet Behaviors of Zn_4Ln_2 (Ln = Dy^{III}, Tb^{III} and Gd^{III}) Complexes with the Multidentate Organic Ligands Formed by Absorption CO_2 in Air through In-situ Reactions

Cheng-Ling Yin,[a] Zhao-Bo Hu,[b] Qiao-Qiao Long,[a] Hui-Sheng Wang,*[,a] Jing Li,[b] You Song,*[,b] Zai-Chao Zhang,[c] Yi-Quan Zhang*[,d] and Zhi-Quan Pan[a]

[a] School of Chemistry and Environmental Engineering, Key Laboratory of Green Chemical Process of Ministry of Education, Wuhan Institute of Technology, Wuhan 430074, P. R. China. E-mail: wangch198201@163.com; Fax: +86-27-87194560

[b] State Key Laboratory of Coordination Chemistry, School of Chemistry and Chemical Engineering, Collaborative Innovation Center of Advanced Microstructures, Nanjing University, Nanjing 210046, P. R. China. E-mail: yousong@nju.edu.cn

[c] Jiangsu Key Laboratory for the Chemistry of Low-dimensional Materials, School of Chemistry and Chemical Engineering, Huaiyin Normal University, P. R. China.

[d] Jiangsu Key Laboratory for NSLSCS, School of Physical Science and Technology, Nanjing Normal University, Nanjing 210023, China. E-mail: zhangyiquan@njnu.edu.cn

*E-mail: wangch198201@163.com (H. -S. Wang), yousong@nju.edu.cn (Y. Song).

Contents

susceptibility data from SQUID magnetometer of compound **2** in the applied field of 2000 Oe.

Table S10. Calculated energy levels (cm^{-1}), $\boldsymbol{g}$ (g_x, g_y, g_z) tensors and m_J values of the lowest eight or seven spin-orbit states of individual Dy^{III} and Tb^{III} fragments of complexes **1** and **2** using CASSCF/RASSI with MOLCAS 8.2

Table S11. Wave functions with definite projection of the total moment | m_J > for the lowest two pin-orbit states of individual Dy^{III} or Tb^{III} fragment of **1** and **2** using CASSCF/RASSI with MOLCAS 8.2.

Table S12. Exchange energies E (cm^{-1}), the tunneling parameter (Δ_{tun}, cm^{-1}) for each exchange doublets and the main values of the g_z for the lowest three exchange doublets of **1** and **2**.

Figure S1. PXRD patterns and simulated patterns generated from single crystal diffraction data for compound **1**

Figure S2. PXRD patterns and simulated patterns generated from single crystal diffraction data for compound **2**

Figure S3. PXRD patterns and simulated patterns generated from single crystal diffraction data for compound **3**

Figure S4. (left**)** Crystal structure of $[Zn_4Gd_2(L_1)_2(L_2)_2(Cl)_2]^{2+}$ of **3**. (right) coordination geometry of Gd^{III} in **3**.

Figure S5. $\chi_M T$ vs T for **3** in a 1000 Oe dc field.

Figure S6. Field dependence of the magnetization for compounds **1-3** at 2 K (top left) and Field dependence of the magnetization for compounds **2** (top right) and **3** (bottom) at different temperatures.

Figure S7. Plots of in-phase (χ_M') versus T (left) and out-of-phase (χ_M'') versus T (right) for complex **1** at zero dc field.

Figure S8. Frequency dependence of the in-phase (χ', left) and out-of-phase (χ'', right) ac signals for **1** (top) and **2** (bottom) under different dc fields at 1.8 K.

Figure S9. Plots of in-phase (χ_M') versus T (left) and out-of-phase (χ_M'') versus T (right) for complex **1** at 1000 Oe dc field.

Figure S10. Plots of in-phase (χ_M') versus T (left) and out-of-phase (χ_M'') versus T (right) for complex **2** at 2000 Oe dc field.

Figure S11. Calculated model structures of individual Dy^{III} and Tb^{III} fragments of complexes **1** and **2**; H atoms are omitted.

Figure S12. The magnetization blocking barriers for individual Dy^{III} or Tb^{III} fragment in **1** and **2**.

Figure S13. Calculated (red solid line) and experimental (black circle dot) data of magnetic susceptibilities of **1** and **2**.

Table S1. The effective energy barriers (U_{eff}) of the selected Zn–Dy clusters, which were obtained through using the Arrhenius law.

Molecular formula	U_{eff} (K)	Molecular formula	U_{eff} (K)
$[(L_AZnBrDy(ovan)(NO_3)(H_2O)]$[18b]	82.9	$[(L^1_EZnBr)_2Dy(MeOH)_2](ClO_4)$[18b]	44.3
$[L_AZnClDy(thd)_2]$[19]	69.3	$[Zn(\mu\text{-}L_F)(\mu\text{-}OAc)Dy(NO_3)_2]$[26a]	41.55
$\{(\mu_3\text{-}CO_3)_2[Zn(\mu\text{-}L_B)Dy(NO_3)]_2\}$[20b]	68	$[ZnDy(HL_D)(NO_3)(OAc)(CH_3OH)](NO_3)$[17]	35.08
$[Zn^{II}_2(L_C)_2(PhCOO)_2Dy^{III}_2(hfac)_4]$[20c]	47.9	$[Zn(\mu\text{-}L_G)(\mu\text{-}OAc)Dy(NO_3)_2]$[20a]	19.1
$[Zn_2Dy(L_D)(NO_3)_2(OAc)_2(H_2O)]$[17]	46.92		

H_2L_A = N, N′-2,2-dimethylpropylenedi(3-methoxysalicylideneiminato);
ovanH = ortho-vanillin;
thd = 2,2,6,6-tetramethyl-3,5-heptanedionato ligand;
H_2L_B = N,N′,N″-trimethyl-N,N″-bis(2-hydroxy-3-methox y -5-methylbenzyl)-diethylenetriamine;
H_2L_C = N,N′-dimethyl-N,N′-bis(2-hydroxy-3,5-dimethylbenzyl)ethylenediamine;
L^1_E = 2-{(E)-[(3-{[(2E,3E)-3-(hydroxyimino)-butan-2-ylidene]amino}-2,2-dimethylpropyl)imino] methyl}-6-methoxyphenol;
H_2L_F = N,N'-dimethyl-N,N'-bis(2-hydroxy-3-formyl-5-bromobenzyl)ethylenediamine;
H_2L_G = N, N', N"-trimethyl-N, N"-bis(2-hydroxy-3-methoxy-5-methylbenzyl)diethylene triamine.

Table S2 Crystal Data and Structure Refinement Parameters for complexes **1-3**

Compounds	**1**	**2**	**3**
formula	$C_{82}H_{94}Cl_2Dy_2N_{18}O_{22}Zn_4$	$C_{82}H_{94}Cl_5N_{15}O_{22}Tb_2Zn_5$	$C_{82}H_{94}Cl_5N_{15}O_{22}Gd_2Zn_5$
formula weight	2341.13	2463.66	2460.32
temperature	296(2) K	173(2)	172(2)
wavelength (Å)	0.71073	0.71073	0.71073
crystal system	monoclinic	monoclinic	monoclinic
space group	$P2_1/n$	$C2/c$	$C2/c$
a (Å)	15.585(2)	31.7901(10)	31．9019(14)
b [Å]	14.9255(19)	19.3393(8)	19.2849(9)
c [Å]	22.836(3)	20.8912(13)	20．9039(8)
α [°]	90	90	90
β [°]	101.876(3)	124.820(10)	124.8110(10)
γ [°]	90	90	90

V [Å^3]	5198.3(12)	10544.2(9)	10559.1(8)
Z	2	4	4
D_c [g/cm^{-3}]	1.496	1.552	1.548
μ (Mo Kα) [mm^{-1}]	2.449	2.637	2.549
F(000)	2348	4928	4920
crystal size (mm)	0.36 × 0.21 × 0.19	0.17× 0.13 × 0.11	0.71× 0.12 × 0.06
θ range (°)	2.23~22.82	3.1223~25.3708	3.076~24.997
index ranges	−18 ≤ h ≤ 18	−37≤ h ≤ 38	−37≤ h ≤ 37
	−12 ≤ k ≤ 17	−23≤ k ≤ 23	-22≤ k ≤ 18
	−25≤ l≤ 27	−25≤ l ≤ 25	-24≤ l ≤ 24
reflections collected	27463	33121	29732
unique reflections [R_{int}]	9394 [0.0866]	9560 [0.0548]	9155[0.0996]
reflections with I > 2σ(I)	4828	6800	5401
goodness-of-fit on F^2	1.099	1.090	1.092
final R indices [I>2sigma(I)]	R_1[a] = 0.0932, wR_2[b] = 0.1901	R_1[a] = 0.0618, wR_2[b] =0.1177	R_1[a] = 0.0720, wR_2[b] =0.1274
R indices (all data)	R_1 = 0.1900 , wR_2 = 0.2099	R_1 = 0.0995, wR_2 = 0.1297	R_1 = 0.1391, wR_2 = 0.1423
S (all data)	1.110	1.194	1.094
$(\Delta\rho)_{max,min}$/e Å^{-3}	2.624 and -1.815	2.669 and -1.727	1.949 and -1.627

[a]$R_1 = \Sigma(||F_o| - |F_c||)/\Sigma|F_o|$. [b] w$R_2 = [\Sigma[w(F_o^2 - F_c^2)^2]/\Sigma[w(F_o^2)^2]]^{1/2}$, $w = 1/[\sigma^2(F_o^2) + [(ap)^2 + bp]$, where $p = [\max(F_o^2, 0) + 2F_c^2]/3$.

Table S3. Selected bond lengths (Å) and angles (°) for **1**.

Bond lengths for **1**			
Dy1-O2	2.292(9)	Dy1-Zn2	3.4896(17)
Dy1-O5	2.303(8)	Zn1-O9	1.979(10)
Dy1-O10	2.306(10)	Zn1-O1	2.021(10)
Dy1-O6	2.332(10)	Zn1-O2	2.028(10)
Dy1-O1	2.325(9)	Zn1-N3	2.062(13)
Dy1-O7	2.568(9)	Zn1-N2	2.099(14)
Dy1-O3	2.600(11)	Zn2-N5	1.969(14)
Dy1-O4	2.631(10)	Zn2-N7	1.984(12)
Dy1-O8	2.768(10)	Zn2-O5	2.022(9)
Dy1-Zn1	3.3696(18)	Zn2-O6	2.071(8)
Bond angles for **1**			
O2-Dy1-O5	136.4(3)	O10-Dy1-O4	83.1(3)
O2-Dy1-O10	75.9(3)	O6-Dy1-O4	70.2(4)
O5-Dy1-O10	84.0(3)	O1-Dy1-O4	129.3(3)
O2-Dy1-O6	109.4(3)	O5-Dy1-O8	127.8(3)
O5-Dy1-O6	67.3(3)	O10-Dy1-O8	141.8(3)
O10-Dy1-O6	143.6(3)	O9-Zn1-O1	101.8(4)
O2-Dy1-O1	69.4(3)	O1-Zn1-O2	81.0(4)
O6-Dy1-O1	138.5(4)	O9-Zn1-N3	121.5(5)
O2-Dy1-O7	140.8(3)	O1-Zn1-N3	135.4(5)
O5-Dy1-O7	64.3(3)	O2-Zn1-N3	85.9(5)
O7-Dy1-O3	71.5(3)	O9-Zn1-N2	107.8(5)
O2-Dy1-O4	60.5(3)	O1-Zn1-N2	94.9(5)
O5-Dy1-O4	79.2(3)		

Symmetry code: a 1-x, -y, -z

Table S4. Selected bond lengths (Å) and angles (°) for **2**.

Bond lengths for **2**			
N2-Zn1	2.102(7)	O3-Tb1	2.605(5)
N3-Zn1	2.043(7)	O4-Tb1	2.622(6)
N4-Zn2	2.193(6)	O5-Zn2	2.035(5)
N5-Zn2	2.033(6)	O5-Tb1	2.349(5)
N6-C41	1.345(10)	O6-Zn2	2.097(5)
O1-Zn1	2.035(5)	O6-Tb1	2.335(5)
O1-Tb1	2.353(5)	O7-Tb1	2.585(5)
O2-Zn1	2.048(6)	O8-Tb1	2.709(5)
O2-Tb1	2.311(5)	O9-Zn1	1.951(5)
Bond angles for **2**			
O10-Tb1-O6	143.70(18)	O9-Zn1-O1	102.9(2)
O2-Tb1-O5	137.38(18)	O9-Zn1-N3	118.3(3)
O10-Tb1-O5	82.89(17)	O1-Zn1-N3	137.7(3)
O6-Tb1-O5	66.48(17)	O9-Zn1-O2	96.8(2)
O2-Tb1-O1	68.20(19)	O1-Zn1-O2	79.7(2)
O10-Tb1-O1	77.72(18)	N3-Zn1-O2	86.0(3)
O6-Tb1-O1	138.57(18)	O9-Zn1-N2	106.9(3)
O5-Tb1-O7	63.39(17)	O1-Zn1-N2	94.7(3)
O1-Tb1-O3	62.30(17)	N5-Zn2-O5	132.7(2)
O7-Tb1-O3	71.96(17)	N5-Zn2-O6	86.5(2)
O2-Tb1-O4	61.88(18)	O5-Zn2-O6	76.79(19)
O10-Tb1-O4	85.01(19)	N5-Zn2-N4	82.0(2)
O6-Tb1-O4	71.28(18)	N4-Zn2-Cl1	104.34(18)
O5-Tb1-O4	79.81(17)		

Symmetry code: a 1.5-x, 0.5-y, 1-z

Table S5. Selected bond lengths (Å) and angles (°) for **3**.

Bond lengths for **3**			
Gd1-O10	2.329(10)	N2-Zn1	2.015(13)
Gd1-O5	2.332(10)	N3-Zn2	2.052(13)
Gd1-O2	2.359(9)	N4-Zn2	2.109(14)
Gd1-O1	2.370(8)	O1-Zn1	2.032(9)
Gd1-O6	2.376(9)	O2-Zn1	2.096(8)
Gd1-O3	2.582(10)	O5-Zn2	2.059(11)
Gd1-O8	2.607(9)	O6-Zn2	2.047(9)
Gd1-O7	2.646(10)	O9-Zn2	1.953(10)
Gd1-O4	2.707(9)	Zn2-O6	2.047(9)
Gd1-Zn2	3.4113(18)	Zn2-N3	2.052(13)
Gd1-Zn1	3.5462(17)	Zn2-O5	2.059(11)
N1-Zn1	2.185(11)	Zn2-N4	2.109(14)
Bond angles for **3**			
O10-Gd1-O5	76.4(4)	O6-Gd1-O4	85.2(3)
O10-Gd1-O2	143.6(3)	O3-Gd1-O4	135.4(3)
O5-Gd1-O2	112.7(3)	O8-Gd1-O4	64.2(3)
O10-Gd1-O1	83.1(3)	O7-Gd1-O4	82.4(3)
O5-Gd1-O1	137.5(3)	N2-Zn1-O1	132.7(4)
O2-Gd1-O1	137.5(3)	N2-Zn1-O2	86.4(4)
O10-Gd1-O6	77.8(3)	O1-Zn1-O2	77.8(4)
O5-Gd1-O6	68.6(3)	N2-Zn1-N1	81.6(5)
O2-Gd1-O6	138.6(3)	O1-Zn1-N1	88.5(4)
O8-Gd1-O7	144.6(3)	O9-Zn2-N3	118.2(5)
O10-Gd1-O4	144.6(3)	O6-Zn2-N3	137.8(5)
O5-Gd1-O4	68.4(3)	O9-Zn2-O5	97.2(4)
O2-Gd1-O4	60.1(3)	O6-Zn2-O5	80.5(4)

Symmetry code: a 1-x, 0.5+y, 0.5-z

Table S6. The possible geometries of nona-coordination metal centers.

Geometry	Point group	Polyhedron
EP-9	D9h	Enneagon
OPY-9	C8v	Octagonal pyramid
HBPY-9	D7h	Heptagonal bipyramid
JTC-9	C3v	Triangular cupola (J3) = trivacant cuboctahedron
JCCU-9	C4v	Capped cube (Elongated square pyramid, J8)
6CCU-9	C4v	Capped cube
JCSAPR-9	C4v	Capped sq. antiprism (Gyroelongated square pyramid J10)
CSAPR-9	C4v	Capped square antiprism
JTCTPR-9	D3h	Tricapped trigonal prism (J51)
TCTPR-9	D3h	Tricapped trigonal prism
JTDIC-9	C3v	Tridiminished icosahedron (J63)
HH-9	C2v	Hula-hoop
MFF-9	Cs	Muffin

Table S7. Deviation parameters from each ideal polyhedron for complexes **1**, **2** and **3**.

	Complex **1**	Complex **2**	Complex **3**
Geometry	Dy1	Tb1	Gd1
EP-9	35.512	35.978	35.857
OPY-9	22.100	21.815	21.703
HBPY-9	16.245	15.884	15.847
JTC-9	15.043	14.591	14.593
JCCU-9	9.573	9.634	9.527
CCU-9	8.395	8.365	8.269
JCSAPR-9	3.286	3.156	3.187
CSAPR-9	1.735	1.668	1.703
JTCTPR-9	5.063	4.831	4.857
TCTPR-9	2.618	2.400	2.414
JTDIC-9	11.558	11.249	11.229
HH-9	10.653	10.533	10.506
MFF-9	1.569	1.627	1.626

Table S8. Best fitted parameters obtained for the extended Debye model with ac susceptibility data from SQUID magnetometer of compound **1** in the applied field of 1000 Oe.

	T(K)	χ_S	χ_T	τ (s)	α	Residual
1	1.8	0.27674	2.60853	0.08368	0.39988	0.00452
2	2.1	0.26071	2.2381	0.06408	0.36573	0.00433
3	2.4	0.23423	1.98145	0.05066	0.37446	0.00301
4	2.7	0.23794	1.58804	0.0284	0.27765	0.00265
5	3.0	0.21357	1.48847	0.02126	0.28496	0.00208
6	3.3	0.19948	1.33665	0.01298	0.25554	0.00112
7	3.6	0.17688	1.21373	0.00806	0.2606	0.00209
8	3.9	0.1684	1.12069	0.00486	0.23499	6.37E-04
9	4.2	0.1538	1.05467	0.003	0.24142	4.85E-04
10	4.4	0.13772	1.00167	0.00212	0.25673	3.09E-04
11	4.6	0.11128	0.96711	0.00145	0.28989	4.54E-04
12	4.8	0.12696	0.92362	0.00149	0.27109	0.00353
13	5.0	0.09014	0.89098	7.23E-04	0.32145	7.06E-04
14	5.2	0.03432	0.88251	4.76E-04	0.38927	9.50E-04
15	5.4	0.05227	0.84125	3.47E-04	0.36722	3.14E-04
16	5.6	0.01583	0.81744	2.36E-04	0.3934	0.00153
17	5.8	2.49E-15	0.792	1.53E-04	0.41555	2.57E-04
18	6.0	4.00E-15	0.77098	1.09E-04	0.43739	5.14E-04
19	6.2	5.15E-15	0.75199	7.82E-05	0.44944	4.52E-04
20	6.4	7.68E-15	0.72876	5.40E-05	0.47147	9.25E-04
21	6.6	1.30E-14	0.69587	3.99E-05	0.45355	5.16E-04
22	7.0	2.39E-14	0.66598	1.80E-05	0.50783	0.00115
23	7.5	3.11E-14	0.62099	8.61E-06	0.51567	8.73E-05
24	8.0	2.84E-14	0.58442	1.07E-05	0.43988	9.33E-04
25	8.5	2.96E-14	0.55082	1.40E-05	0.36124	0.00203
26	9.0	3.82E-14	0.52891	1.41E-05	0.37713	0.00239

Table S9. Best fit parameters obtained for the extended Debye model with ac susceptibility data from SQUID magnetometer of compound **2** in the applied field of 2000 Oe.

	T(K)	χ_S	χ_T	τ (s)	α	Residual
1	1.8	0.1460	1.5200	2.63E-03	0.4009	3.80E-03
2	2.2	0.1310	1.3900	2.68E-03	0.4153	4.01E-03
3	2.6	0.1450	1.2900	2.48E-03	0.3737	1.13E-02
4	3	0.1430	1.1500	2.12E-03	0.333	1.45E-03
5	3.4	0.1470	1.0600	1.92E-03	0.2951	1.68E-03
6	3.8	0.1460	0.9940	1.83E-03	0.2732	5.70E-03
7	4.2	0.1490	0.8830	1.56E-03	0.2225	3.50E-03
8	4.6	0.1450	0.8320	1.48E-03	0.2088	3.81E-03
9	5	0.1350	0.7890	1.40E-03	0.2161	4.14E-03
10	5.4	0.1320	0.7100	1.21E-03	0.1845	2.60E-03
11	5.8	0.1250	0.6770	1.15E-03	0.1889	2.94E-03
12	6.2	0.1260	0.6260	1.05E-03	0.1625	2.40E-03
13	6.6	0.1200	0.5910	9.59E-04	0.1584	2.63E-03
14	7	0.1120	0.5580	8.76E-04	0.1594	1.61E-03
15	8	0.1020	0.4970	7.17E-04	0.1499	1.35E-03
16	8.5	0.1000	0.4670	6.46E-04	0.1396	9.41E-04
17	9	0.0930	0.4450	5.76E-04	0.1465	6.43E-04
18	9.5	0.0884	0.4230	5.16E-04	0.141	5.49E-04
19	10	0.0882	0.4010	4.59E-04	0.1372	4.30E-04
20	11.4	0.0762	0.3500	3.25E-04	0.1167	1.93E-04
21	11.8	0.0765	0.3380	2.95E-04	0.1143	1.52E-04
22	12.2	0.0777	0.3260	2.71E-04	0.0977	1.66E-04
23	12.6	0.0638	0.3170	2.30E-04	0.1132	1.20E-04
24	13	0.0710	0.3080	2.12E-04	0.1119	1.34E-04
25	13.4	0.0632	0.3000	1.81E-04	0.1201	7.16E-05
26	13.8	0.0639	0.2920	1.59E-04	0.1164	5.65E-05
27	14.2	0.0860	0.2910	1.72E-04	0.1008	1.96E-04

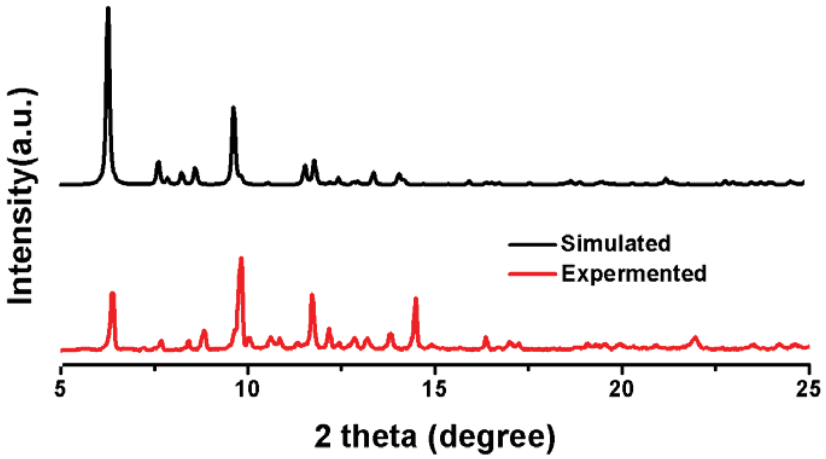

Figure S1. PXRD patterns and simulated patterns generated from single crystal diffraction data for compound **1**

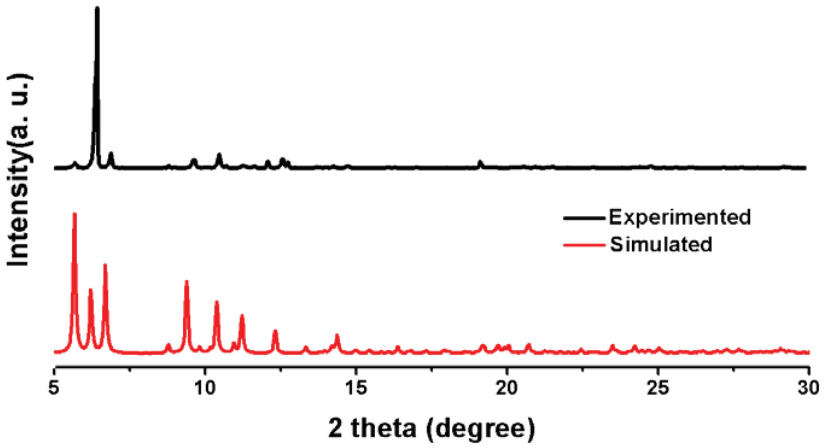

Figure S2. PXRD patterns and simulated patterns generated from single crystal diffraction data for compound **2**

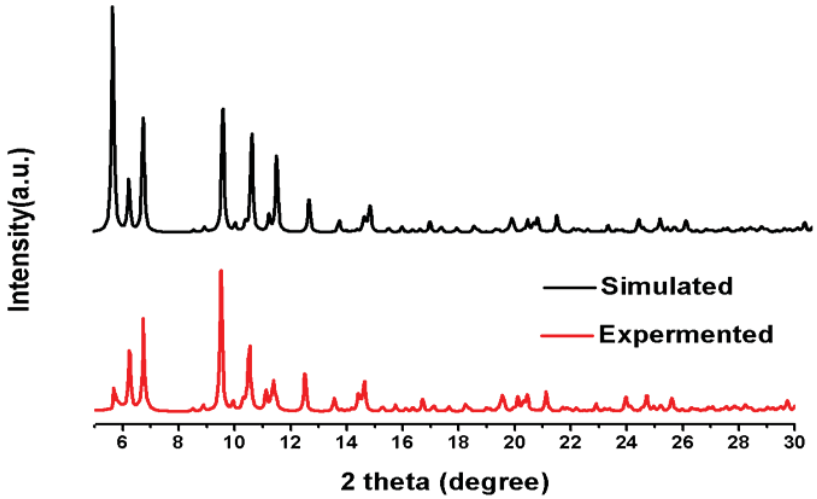

Figure S3. PXRD patterns and simulated patterns generated from single crystal diffraction data for compound **3**

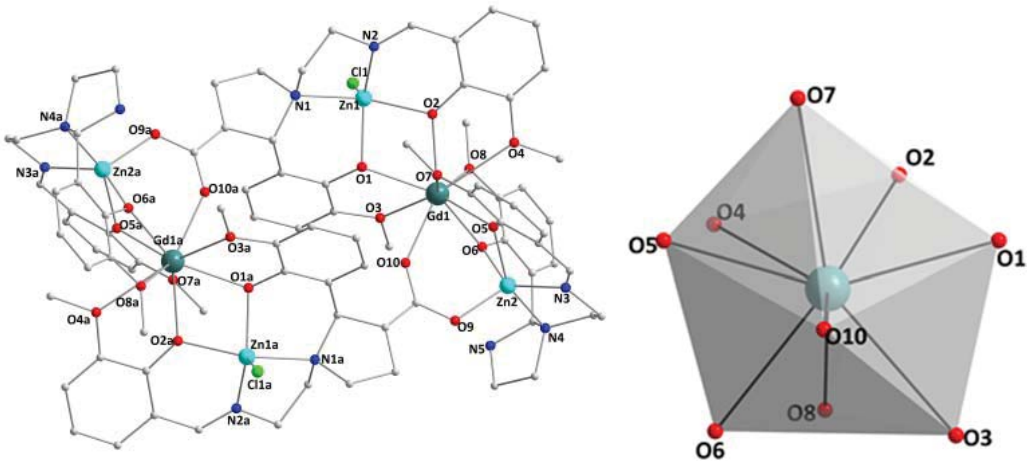

Figure S4. (left**)** Crystal structure of $[Zn_4Gd_2(L_1)_2(L_2)_2(Cl)_2]^{2+}$ of **3**. For clarity, the H atoms are omitted (symmetry code: a 1-x, 0.5+y, 0.5-z). (right) coordination geometry of Gd^{III} in **3**.

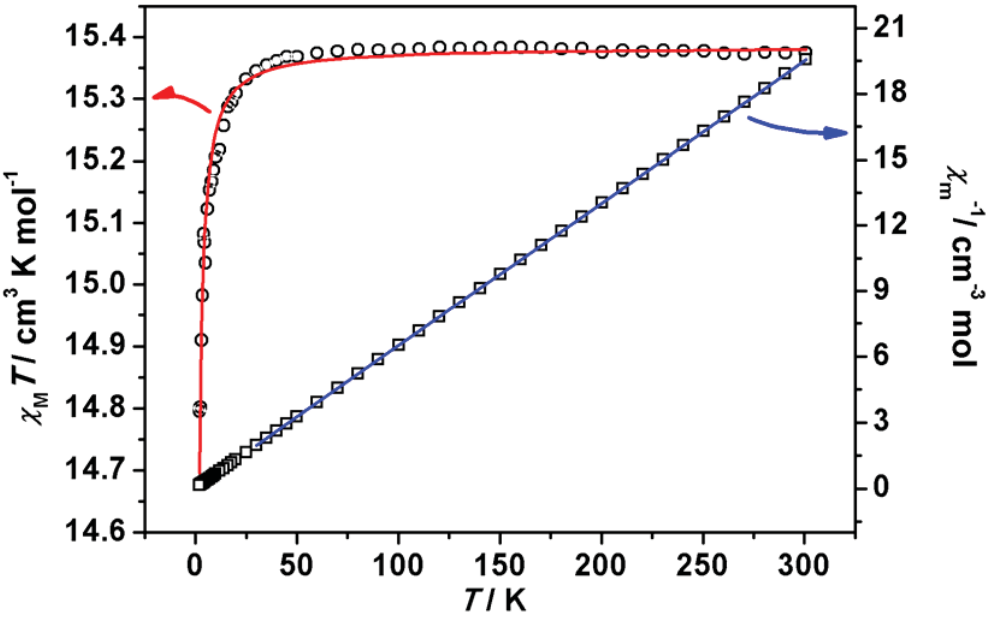

Figure S5. $\chi_M T$ vs T for **3** in a 1000 Oe dc field. The red solid and blue solid lines represent the fitted results by PHI program and using the Curie–Weiss equation $1/\chi_M = (T-\vartheta)/C$, respectively.

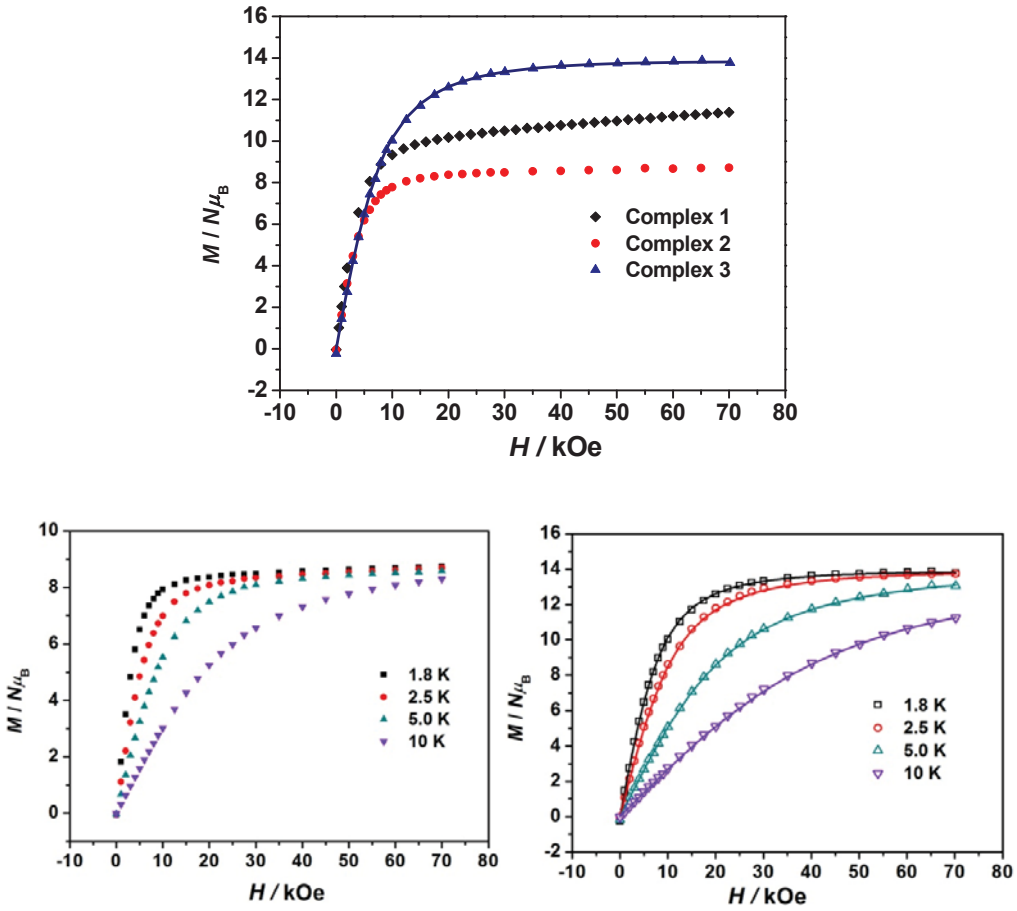

Figure S6. Field dependence of the magnetization for compounds **1-3** at 1.8 K (top), and the plots of the field dependence of the magnetization for compounds **2** (bottom left) and **3** (bottom right) at different temperatures. Solid lines represent the fitted results for **3** by PHI program.

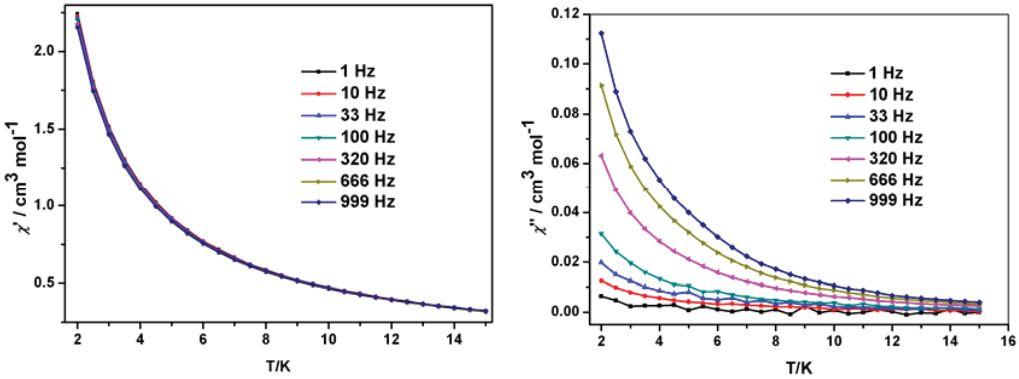

Figure S7. Plots of in-phase (χ_M') versus T (left) and out-of-phase (χ_M'') versus T (right) for complex **1** at zero dc field.

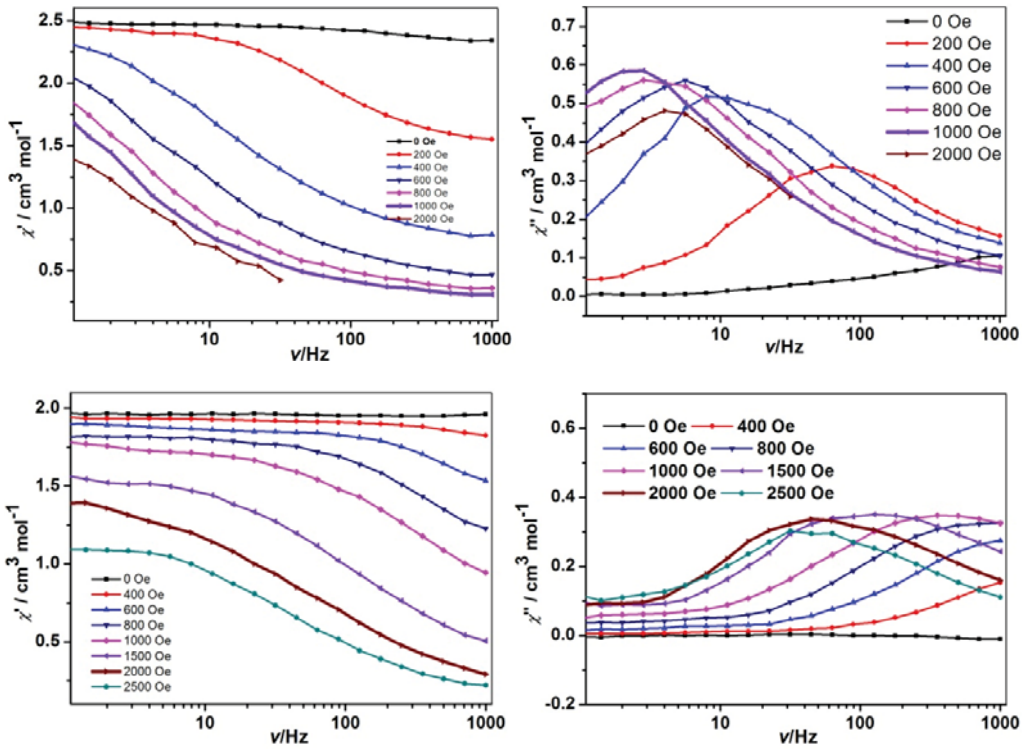

Figure S8. Frequency dependence of the in-phase (χ', left) and out-of-phase (χ'', right) ac signals for **1** (top) and **2** (bottom) under different dc fields at 1.8 K. To see easily, the χ' and χ'' ac susceptibility signals at optimal dc field used in this work were represented by thick lines, which indicate that the optimal dc fields for **1** and **2** were 1000 Oe and 2000 Oe, respectively.

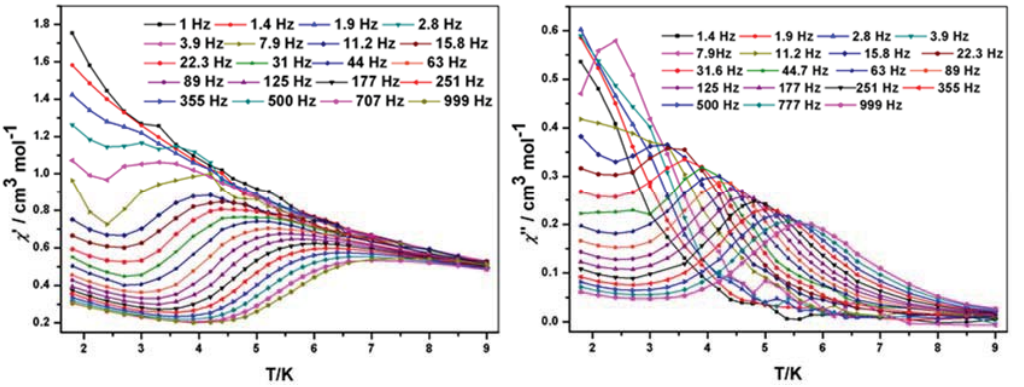

Figure S9. Plots of in-phase (χ_M') versus T (left) and out-of-phase (χ_M'') versus T (right) for complex **1** at 1000 Oe dc field.

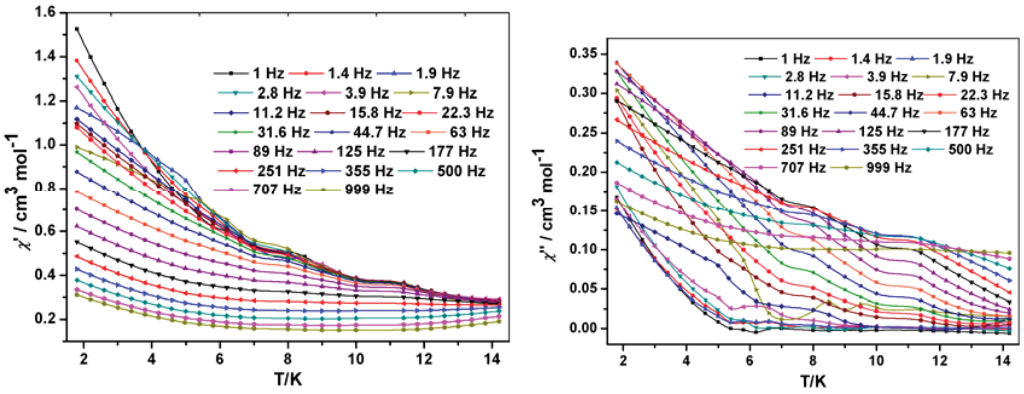

Figure S10. Plots of in-phase (χ_M') versus *T* (left) and out-of-phase (χ_M'') versus *T* (right) for complex **2** at 2000 Oe dc field.

Computational details

Mononuclear complexes **1** and **2** have one type of Dy^{III} and Tb^{III} fragments, respectively, and thus only one individual Dy^{III} or Tb^{III} fragment for them was calculated. Complete-active-space self-consistent field (CASSCF) calculations on individual Dy^{III} and Tb^{III} fragments (see Figure S1 for the calculated model structures of individual Dy^{III} and Tb^{III} fragments; see Figure S4 for the complete structures of complexes **1** and **2**) extracted from the compounds on the basis of single-crystal X-ray determined geometry have been carried out with MOLCAS 8.2[S1] program package.

The basis sets for all atoms are atomic natural orbitals from the MOLCAS ANO-RCC library: ANO-RCC-VTZP for Dy^{III} or Tb^{III} ion; VTZ for close O; VDZ for distant atoms. The calculations employed the second order Douglas-Kroll-Hess Hamiltonian, where scalar relativistic contractions were taken into account in the basis set and the spin-orbit couplings were handled separately in the restricted active space state interaction (RASSI-SO) procedure. Active electrons in 7 active spaces include all *f* electrons (CAS(9 in 7) for individual Dy^{III} fragmet and CAS(8 in 7) for individual Tb^{III} fragment in the CASSCF calculation. To exclude all the doubts, we calculated all the roots in the active space. We have mixed the maximum number of spin-free state which was possible with our hardware (all from 21 sextets, 128 from 224 quadruplets, 130 from 490 doublets for individual Dy^{III} fragmet; all from 7

septets, all from 140 quintets and 68 from 500 triplets for individual Tb^{III} fragment). Single_Aniso[S2] program was used to obtain the energy levels, ***g*** tensors, m_J values, magnetic axes, *et al.*, based on the above CASSCF/RASSI calculations.

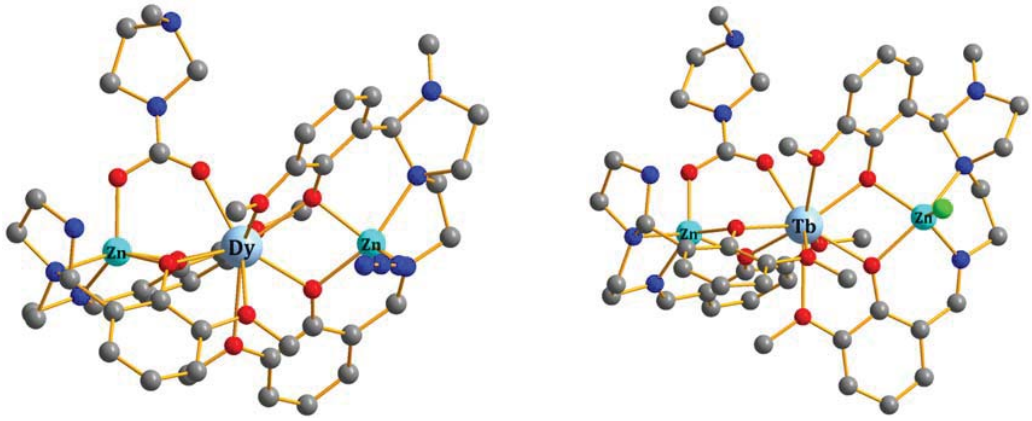

1 **2**

Figure S11. Calculated model structures of individual Dy^{III} and Tb^{III} fragments of complexes **1** and **2**; H atoms are omitted.

Table S10. Calculated energy levels (cm^{-1}), ***g*** (g_x, g_y, g_z) tensors and m_J values of the lowest eight or seven spin-orbit states of individual Dy^{III} and Tb^{III} fragments of complexes **1** and **2** using CASSCF/RASSI with MOLCAS 8.2.

	1 (Dy^{III})			**2** (Tb^{III})		
	E/cm^{-1}	***g***	m_J	E/cm^{-1}	***g***	m_J
1	0.0	0.007 0.013 19.349	±15/2	0.0 0.01	0.000 0.000 17.908	±6
2	93.4	0.218 0.371 15.875	±13/2	177.4 178.7	0.000 0.000 14.547	±5
3	145.8	0.352 0.834 13.332	±11/2	281.5		0
4	236.4	0.641	±9/2	305.9	0.000	±3

		1.703 11.804		319.8	0.000 6.156	
KD5	322.6	0.026 1.825 11.216	±7/2	383.6 397.3	0.000 0.000 10.492	±4
KD6	394.9	3.837 5.143 8.824	±5/2	497.0 500.2	0.000 0.000 14.345	±2
KD7	497.1	1.324 2.611 12.271	±1/2	640.8 641.8	0.000 0.000 17.561	±1
KD8	569.7	0.732 3.173 17.014	±3/2			

Table S11. Wave functions with definite projection of the total moment | m_J > for the lowest two pin-orbit states of individual Dy^{III} or Tb^{III} fragment of **1** and **2** using CASSCF/RASSI with MOLCAS 8.2.

		E/cm^{-1}	wave functions
1	Dy^{III}	0.0	91%|±15/2>+7%|±11/2>
		93.4	60%|±13/2>+6%|±11/2>+22%|±9/2>+6%|±7/2>+4%|±5/2>
2	Tb^{III}	0.0	100%|±6>
		0.01	
		177.4	95%|±5>
		178.7	

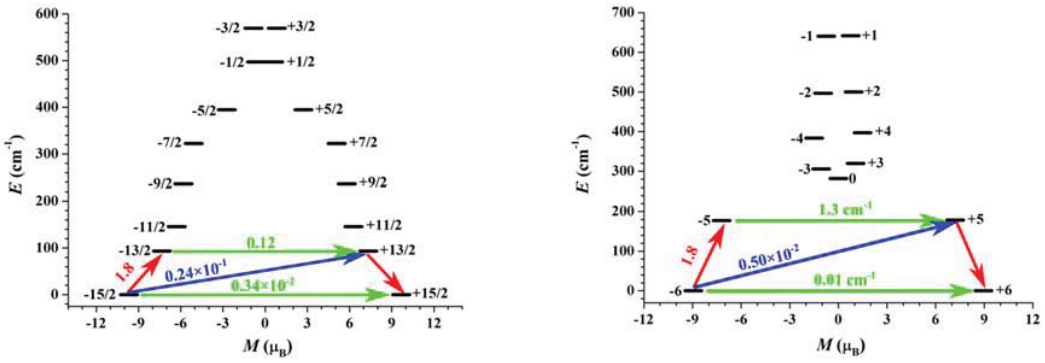

1(Dy^{III} **)** **2**(Tb^{III})

Figure S12. The magnetization blocking barriers for individual Dy^{III} or Tb^{III} fragment in **1** and **2**. The thick black lines represent the spin-orbit states of individual Dy^{III} or Tb^{III} fragment as a function of their magnetic moment along the magnetic axis. The green lines correspond to the diagonal matrix element of the transversal magnetic moment; the blue lines represent Orbach relaxation processes. The path shown by the red arrows represents the most probable path for magnetic relaxation in the corresponding compounds. The numbers at each arrow stand for the mean absolute value of the corresponding matrix element of transition magnetic moment.

To fit the exchange interactions in **1** and **2**, we took two steps to obtain them. Firstly,

we calculated individual Dy^{III} and Tb^{III} fragments using CASSCF to obtain the corresponding magnetic properties. Then, the exchange interaction between the magnetic centers is considered within the Lines model,[S3] while the account of the dipole-dipole magnetic coupling is treated exactly. The Lines model is effective and has been successfully used widely in the research field of *f*-element single-molecule magnets.[S4]

For **1** and **2**, there is only one type of *J*.

The exchange Ising Hamiltonian are:

$$\hat{H}_{exch} = -\tilde{J}\,\hat{\tilde{S}}_{Dy1}\,\hat{\tilde{S}}_{Dy2} \quad \text{(S1)}$$

$$\hat{H}_{exch} = -\tilde{J}\,\hat{\tilde{S}}_{Tb1}\,\hat{\tilde{S}}_{\mathrm{Tb2}} \quad \text{(S2)}$$

The $\tilde{J}_{total}$ is the parameter of the total magnetic interaction ($\tilde{J}_{total} = \tilde{J}_{diploar} + \tilde{J}_{exchange}$) between magnetic center ions. The $\tilde{S}_{Dy}$ = ±1/2 and $\tilde{S}_{Tb}$ = ±1/2 are the ground pseudospin on the Dy^{III} and Tb^{III} sites, respectively. The dipolar magnetic coupling can be calculated exactly, while the exchange coupling constants were fitted through comparison of the computed and measured magnetic susceptibilities using the Poly_Aniso program.[S2]

Table S12. Exchange energies *E* (cm^{-1}), the tunneling parameter (Δ_{tun}, cm^{-1}) for each exchange doublets and the main values of the g_z for the lowest three exchange doublets of **1** and **2**.

	1			**2**		
	E	Δ_{tun}	g_{zz}	*E*	Δ_{tun}	g_{zz}
1	0.0	0.56×10^{-8}	0.000	0.0	0.42×10^{-3}	35.725
2	0.2	0.12×10^{-6}	38.698	0.1	0.41×10^{-3}	0.000
3	93.4	0.10×10^{-4}	0.000	177.4	0.14×10^{-1}	18.896

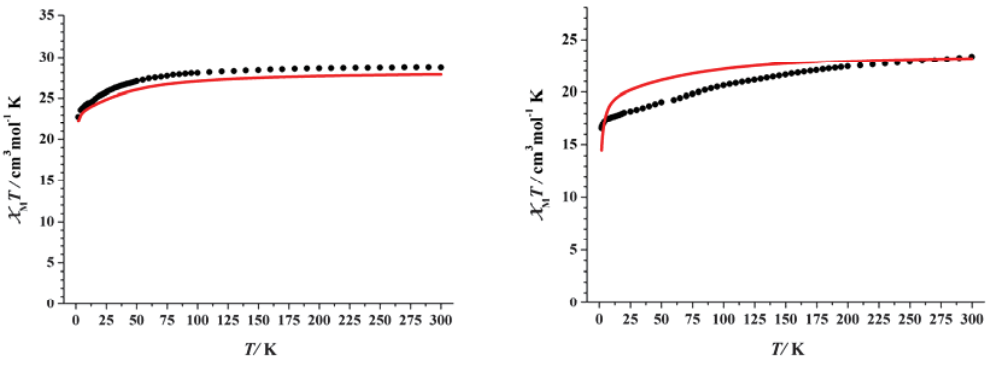

1 **2**

Figure S13. Calculated (red solid line) and experimental (black circle dot) data of magnetic susceptibilities of **1** and **2**. The intermolecular interactions *zJ´* of **1** and **2** were fitted to 0.00 cm^{-1} and −0.03 cm^{-1}, respectively.

References:

S1 (a) Aquilante, F.; De Vico, L.; Ferré, N.; Ghigo, G.; Malmqvist, P.-Å.; Neogrády, P.; Pedersen, T. B.; Pitonak, M.; Reiher, M.; Roos, B. O.; Serrano-Andrés, L.; Urban, M.; Veryazov, V.; Lindh, R. *J. Comput. Chem.*, **2010**, *31*, 224. (b) Veryazov, V.; Widmark, P. -O.; Serrano-Andres, L.; Lindh, R.; Roos, B. O. *Int. J. Quantum Chem.*, **2004**, *100*, 626. (c) Karlström, G.; Lindh, R.; Malmqvist, P. -Å.; Roos, B. O.; Ryde, U.; Veryazov, V.; Widmark, P. -O.; Cossi, M.; Schimmelpfennig, B.; Neogr´ady, P.; Seijo, L. *Comput. Mater. Sci*., **2003**, *28*, 222.

S2 (a) Chibotaru, L. F.; Ungur, L.; Soncini, A. *Angew. Chem. Int. Ed.*, **2008**, *47*, 4126. (b) Ungur, L.; Van den Heuvel, W.; Chibotaru, L. F. *New J. Chem.*, **2009**, *33*, 1224. (c) Chibotaru, L. F.; Ungur, L.; Aronica, C.; Elmoll, H.; Pilet, G.; Luneau, D. *J. Am. Chem. Soc.*, **2008**, *130*, 12445.

S3 Lines, M. E. *J. Chem. Phys*. **1971**, *55*, 2977.

S4 (a) Mondal, K. C.; Sundt, A.; Lan, Y. H.; Kostakis, G. E.; Waldmann, O.; Ungur, L.; Chibotaru, L. F.; Anson, C. E.; Powell, A. K. *Angew. Chem. Int. Ed*. **2012**, *51*, 7550. (b) Langley, S. K.; Wielechowski, D. P.; Vieru, V.; Chilton, N. F.; Moubaraki, B.; Abrahams, B. F.; Chibotaru, L. F.; Murray, K. S. *Angew. Chem. Int. Ed*. **2013**, *52*, 12014.